



Available at
<http://pvamu.edu/aam>
Appl. Appl. Math.
ISSN: 1932-9466

Applications and Applied
Mathematics:
An International Journal
(AAM)

Vol. 4, Issue 2 (December 2009), pp. 249 – 262
(Previously, Vol. 4, No.2)

Spatial Instability of Electrically Driven Jets with Finite Conductivity and Under Constant or Variable Applied Field

Saulo Orizaga and Daniel N. Riahi

Department of Mathematics
University of Texas-Pan American
1201 West University Drive
Edinburg, Texas 78539-2999 USA
Email: driahi@utpa.edu

Received: May 20, 2009; Accepted: November 12, 2009

Abstract

We investigate the problem of spatial instability of electrically driven viscous jets with finite electrical conductivity and in the presence of either a constant or a variable applied electric field. A mathematical model, which is developed and used for the spatially growing disturbances in electrically driven jet flows, leads to a lengthy equation for the unknown growth rate and frequency of the disturbances. This equation is solved numerically using Newton's method. For neutral temporal stability boundary, we find, in particular, two new spatial modes of instability under certain conditions. One of these modes is enhanced by the strength Ω of the applied field, while the other mode decays with increasing Ω . The growth rates of both modes increase mostly with decreasing the axial wavelength of the disturbances. For the case of variable applied field, we found the growth rates of the spatial instability modes to be higher than the corresponding ones for constant applied field, provided Ω is not too small.

Keywords: Spatial instability, jet flow, electric field, jet instability, flow instability

MSC 2000: 76E25, 76W05

1. Introduction

This paper considers the problem of spatial instability of a cylindrical viscous jet of fluid with finite electrical conductivity and a static charge density and in the presence of an external

constant or variable electric field. The investigations of electrically forced jets are important particularly in applications such as those to electrospinning [Baily (1988)] and electrospinning [Hohman et al. (2001a), (2001b)]. Electrospinning is a technology that uses electric fields to produce and control small fibers. The aim is at producing non-woven materials that are unparalleled in their porosity, high surface area, and the fineness and uniformity of their fibers. Electrospinning is a technology that uses electric field to produce and control sprays of very small drops. The aim is at producing very small drops that are uniform in size and are of charged macromolecules in the gas phase.

Without presence of electrical field effects, it is known for several decades that spatially growing disturbances are, in general, more appropriate and realized than the temporally growing counterparts for the jet flows and other types of free shear flows [Drazin and Reid (1981)]. For example, Michalke (1969) studied instability of the free shear layers and found that theoretical results based on the spatial instability have better agreement with the corresponding experimental results. Later, additional investigations of spatial instability of free shear flows and jets were reported by a number of authors including those by Monkewitz and Huerre (1982), Lie and Riahi (1988), Tam (1993), Soderberg (2003) and Healey (2008). Soderberg (2003) showed, in particular, agreement between the linear spatial instability results and the corresponding experimental results.

For the jet flows driven by the electric forces, temporal instability of such flows has been studied theoretically by several authors [Hohman et al. (2001a), (2001b); Reneker et al. (2000); Shkadov and Shutov (2001), Fridrikh et al. (2003)]. Hohman et al. (2001a) studied the linear temporal instability of an electrically forced jet with uniform applied field. The simplified equations for the dependent variables of the disturbances that they analyzed were based on the long wavelength and asymptotic approximations of the original electro-hydrodynamic equations. For the axisymmetric jets, the authors detected, in particular, two temporal instability modes, and they discussed the properties of such instability modes in the various possible limits. Other investigations of the problems dealing with the electrically forced jets with applications in electrospinning of nanofiber are reported in several papers [Sun et al. (2003), Li and Xia (2004), Yu et al. (2004)].

Very recently Riahi (2009) considered electrically forced jets with variable applied field. He followed a modeling approach analog to that due to Hohman et al. (2001a) and investigated analytically spatial instability of axisymmetric jets under idealistic conditions of either jet of zero electrical conductivity or jet of infinite electrical conductivity and subjected to certain restrictions on the frequency of the disturbances. He detected two spatial modes of instability each of which was enhanced with increasing the strength of the externally imposed applied electric field. These modes existed under certain restricted ranges of the axial wave number of disturbances, but, in particular, did not exist if the axial wave number was sufficiently small.

In the present study we first use a method of approach similar to that employed in Riahi (2009) to arrive at a mathematical model for the non-idealistic (realistic) electrically driven viscous jets with finite conductivity. Next, we consider spatial instability of the jets for externally imposed constant or variable applied field. We then determine a rather lengthy dispersion relation, which relates the growth rate of the spatially growing disturbances to the wave number in the axial

direction, the frequency and the non-dimensional parameters of the model. We solve numerically the dispersion relation for the growth rate and frequency of the disturbances using the Newton's method [Anderson et al. (1984)]. We found a number of interesting results. In particular, for temporally neutral case and in contrast to the results in Riahi (2009), we detect two spatially growing modes in wider range of values in the axial wave number of disturbances, one of which is driven and enhanced by the electric field, while another spatial instability mode decays with increasing the strength of the applied field.

2. Formulation and Analysis

We consider a cylindrical viscous jet of fluid with finite electrical conductivity and a static charge density, which is subjected by an externally imposed constant or variable electric field. We begin with the governing electro-hydrodynamic equations [Melcher and Taylor (1969)] for such a jet flow. These equations are for the mass conservation, momentum, charge conservation and for the electric potential, which are given, respectively, by

$$DP/Dt + \rho \nabla \cdot u = 0, \quad (1a)$$

$$\rho Du/Dt = -\nabla P + \nabla \cdot \nabla(\mu u) + qE, \quad (1b)$$

$$Dq/Dt + \nabla \cdot (KE) = 0, \quad (1c)$$

$$E = -\nabla \Phi, \quad (1d)$$

where $D/Dt \equiv \partial/\partial t + u \cdot \nabla$ is the total derivative, t is the time variable, u is the velocity vector, P is the pressure, E is the electric field vector, Φ is the electric potential, q is the free charge density, ρ is the fluid density, μ is the dynamic viscosity and K is the electrical conductivity of the jet.

The expression for the internal pressure P in the jet given in the momentum equation (1b) is found by balancing across the free boundary of the jet the pressure, viscous forces, capillary forces and the electric energy density plus the radial self-repulsion of the free charges on the free boundary [Melcher and Taylor (1969)], which lead to the following expression for P

$$P = \gamma \kappa - [(\varepsilon - \tilde{\varepsilon})/(8\pi)]E^2 - (4\pi/\tilde{\varepsilon})\sigma^2/\tilde{\varepsilon}, \quad (2)$$

where κ is twice the mean curvature of the interface, $\varepsilon/(4\pi)$ is the permittivity constant in the jet, $\tilde{\varepsilon}/(4\pi)$ is the permittivity constant in the air, γ is the surface tension and σ is the surface free charge.

Following Hohman, et al. (2001a), we consider the fluid jet to be Newtonian and incompressible that moves axially, and the ambient fluid is considered to be passive air. We make use of the governing equations (1) in the cylindrical coordinate system with the origin at the center of the exit section of the jet's nozzle, where the jet flow is emitted, and with the axial z -axis along the axis of the jet. We consider the axisymmetric form of the dependent variables where there are no variations of the dependent variables with respect to the azimuthal variable and with zero azimuthal velocity.

Following the proper approximations due to Hohman et al. (2001a) for a thin and long jet in the axial direction, we assume the length scale in the axial direction to be large in comparison to that in the radial direction and make use of a perturbation expansion in the small jet' aspect ratio. Expanding the dependent variables of the jet in a Taylor series in the radial variable r and using such expansions in the governing equations, we end up with relatively simple equations for the dependent variables as functions of t and z after we keep only the leading terms. Following the method of approach due to Hohman et al. (2001a), we employ (1d) and Coulomb's integral equation to arrive at an equation for the electric field, which is essentially the same as the one given in Hohman et al. (2001a) and will not be repeated here. We then non-dimensionalize these equations using the radius r_0 of the cross-sectional area of the nozzle exit at $z=0$, $E_0 = \{\gamma[(\varepsilon - \tilde{\varepsilon})r_0]\}^{1/2}$, $t_0 = (\rho r_0/\gamma)^{1/2}$, (r_0/t_0) and $(\gamma \tilde{\varepsilon}/r_0)^{1/2}$ as the scales for length, electric field, time, velocity and surface charge, respectively. The resulting non-dimensional equations are then

$$\partial(h^2)/\partial t + \partial(h^2 v)/\partial z = 0, \quad (3a)$$

$$\partial(h\sigma)/\partial t + \partial(hv\sigma)/\partial z + \partial[0.5h^2 E(z) K^* \tilde{K}(z)] = 0, \quad (3b)$$

$$\begin{aligned} \partial v/\partial t + v\partial v/\partial z = & -(\partial/\partial z)\{h [1+(\partial h/\partial z)^2]^{-0.5} - (\partial^2 h/\partial z^2)[1+(\partial h/\partial z)^2]^{-1.5} - E^2/(8\pi) - 4\pi\sigma^2\} \\ & + 2 E\sigma/(h\sqrt{\beta}) + [3v^*/(h^2)](\partial/\partial z)[h^2\partial v/\partial z], \end{aligned} \quad (3c)$$

$$E_b(z) = E - \ln(\chi)[(\beta/2)(\partial^2/\partial z^2)(h^2 E) - 4\pi\sqrt{\beta}(\partial/\partial z)(h\sigma)]. \quad (3d)$$

Here, $v(z, t)$ is the axial velocity, $h(z, t)$ is the radius of the jet' cross-section at the axial location z , $\sigma(z, t)$ is the surface charge, the conductivity K is assumed to be a function of z in the form $K = K_0 \tilde{K}(z)$, where K_0 is a constant dimensional conductivity and $\tilde{K}(z)$ is a non-dimensional variable function, $K^* = K_0 \{\rho r_0^3 / [\gamma \beta (\tilde{\varepsilon})^2]\}^{0.5}$ is the non-dimensional conductivity parameter, $\beta = \varepsilon/\tilde{\varepsilon} - 1$, $v^* = [v^2 \rho / (\gamma r_0)]^{0.5}$ is the non-dimensional viscosity parameter, $E_b(z)$ is an applied electric field and χ is the inverse of a local aspect ratio, which is assumed to be large.

Next, we consider the electrostatic equilibrium solution, which is referred to here as the basic state solution, for the equations (3). The basic state solutions for the dependent variables of the jet designated with a subscript 'b', are given by

$$h_b = 1, v_b = 0, \sigma_b = \sigma_0, E_b = \Omega / \tilde{K}(z) = \Omega \{1 - [8\sigma_0 \pi / (\Omega \sqrt{\beta})]z\}. \quad (4a-d)$$

Here, Ω and σ_0 are constant quantities and σ_0 is the background free charge density. We let $\delta = 8\sigma_0 \pi / (\Omega \sqrt{\beta})$ to be a small parameter ($\delta \ll 1$) and consider a series expansion in powers of δ for all the dependent variables in the case of variable applied field.

In present paper we study the cases where the applied electric field can be either constant ($\delta = 0$) or variable ($\delta \neq 0$). We consider each dependent variable as sum of its basic state solution plus a small perturbation, which is assumed to be oscillatory in both time and axial variables. Thus, we have

$$(h, v, \sigma, E) = (h_b, v_b, \sigma_b, E_b) + (h_1, v_1, \sigma_1, E_1). \quad (5a)$$

Here, the perturbation quantities designated with a subscript ‘1’, are given by

$$(h_1, v_1, \sigma_1, E_1) = (h', v', \sigma', E') \exp[i\omega t + (s + ik)z], \tag{5b}$$

where (h', v', σ', E') are small constants, i is the pure imaginary number $\sqrt{-1}$, ω is the real constant frequency, s is the real growth rate of spatially growing disturbances and k is the axial wave number. Using (4)-(5) in (3), we linearize the resulting equations with respect to the amplitude of the perturbation. We consider the linearized equations to the lowest order in δ (for variable applied field case) and divide each equation by the exponential function $\exp[i\omega t + (s + ik)z]$. We then find four linear algebraic equations for the unknown constants h', v', σ' and E' . To obtain non-trivial (non-zero) values of these constants, the 4×4 determinant of the coefficients of these unknowns must be zero. This leads to the following dispersion relation:

$$\begin{aligned} &0.5(k^2 - 1 - s^2 - 2iks)(k^2 - s^2 - 2iks)(i\omega A + 4\pi K^*/\sqrt{\beta}) \\ &+ (k^2 - s^2 - 2iks) \{i\omega [12\pi v^* K^*/\sqrt{\beta} + \Omega^2/(4\pi)] + \Omega^2 K^* A/\sqrt{\beta}\} \\ &- \omega^2 \{4\pi K^*/\sqrt{\beta} + [i\omega + 3v^*(k^2 - s^2 - 2iks)]A\} \\ &+ (k - is)^2 \{2i\omega A \pi \sigma_0 [1 + 8 \ln(.89k)/(2 + \Lambda)] + (4\pi K^*/\sqrt{\beta}) [2\pi \sigma_0^2 - \Omega \sigma_0 (s + ik)] \\ &\times (4 + 1/\ln(.89k))/((k - is)^2 \sqrt{\beta})\} = 0. \end{aligned} \tag{6}$$

Here, $A = 1 - 2/[\beta(k - is)^2 \ln(1/\chi)]$, $\Lambda = -\beta(k - is)^2 \ln(.89k)$ and $\chi = 1/(0.89k)$ [Hohman et al. (2001a)].

3. Results and Discussion

The dispersion relation (6) is investigated for both variable and constant applied field cases. For variable applied field, where $\delta \neq 0$, we assume that δ is small of order about 0.1, and here both Ω and β cannot take zero value, so that we set $\sigma_0 \leq 0.1$, which turns out to keep the value of δ of order 0.1 in the range of values of the rest of the parameters that are considered in the present study. For constant applied field case, we set $\sigma_0 = 0$. In this section we describe each of the cases that are considered and provide and discuss the corresponding results.

Before presenting the main results and the corresponding discussion for the present study, we explain a connection that we establish between the asymptotic and idealistic results due to Riahi (2009), which was carried out for perfect conductivity ($K^* = \infty$) and variable applied field case, and the corresponding present numerical ones for finite but very large conductivity. We also thought that such a comparison between the previous idealistic work and the present one under such high conductivity regime can serve as a validation for the present numerical code if very good agreement is resulted for such limiting case. We, thus, generated computational data for the parameter regime in Riahi (2009), where $v^* = 0.333$, $\beta = 77.0$ and $\sigma_0 = 0.1$, but for cases of very large conductivity ($K^* \geq 10^5$).

The numerical results, for $K^* > 10^5$ like $K^* = 10^7$ were found to be almost indistinguishable from those for $K^* = 10^5$. Figure 1 presents the result for the growth rate s versus the wave number k

for the two detected electric modes of instability for infinite conductivity in Riahi (2009) (dashed lines) and those found here for $K^* = 10^5$ (dotted lines). It can be seen that the agreement between the present result and the corresponding one in Riahi (2009) is very good. We also checked the corresponding values of the strength of the applied field Ω for both instability modes in the present numerical case and found that they agree very well with the corresponding ones in Riahi (2009) indicating that both instability modes are enhanced with Ω .

For the main computation of the present study, we consider the fluid to be a type of liquid, which can be used in the experimental investigation for validation of the mathematical modeling of the problem such as a type of glycerol in water mixture. For such fluid, we set representative values of the parameters to be $K^* = 19.60$, $\nu^* = 0.61$, $\beta = 77.00$, and $\sigma_0 = 0$ for constant applied field or $\sigma_0 = 0.10$ for variable applied field. We then used (6) to generate data for the growth rates and frequencies for different values of Ω and for both variable and constant applied field cases. The results are briefly presented in the following paragraphs.

For $\Omega = 1$, we found only one mode of instability for both constant and variable applied field cases. The growth rates s and the frequencies ω of disturbances increase with the axial wave numbers k ($0 < k < 1$) of the disturbances. For constant applied field, the growth rates of the disturbances are larger than the corresponding ones for the variable applied field if $0.04 \leq k < 1$, while the opposite holds if $0 < k < .04$. For constant applied field, the frequencies of the disturbances are larger than the corresponding ones for the variable applied field if $0 < k \leq 0.96$, while the opposite holds if $0.96 < k < 1$. We classify this mode of instability, which also exists for $\Omega < 1$, as a spatial analog of the well-known surface tension driven Rayleigh mode of instability that can break-up a liquid jet in air [Rayleigh (1879); Drazin and Reid (1981)]. Hereafter, we refer to this mode as spatial Rayleigh mode (SRM).

For $\Omega = 1.5$, we found SRM to be the only mode of instability for both constant and variable applied field cases. The growth rates s and the frequencies ω of the disturbances again increase with k . For constant applied field, s is larger than the corresponding one for the variable field if $0.12 \leq k < 1$, while the opposite holds if $0 < k < 0.12$. For constant applied field, ω is larger than the corresponding one for the variable applied field if $0 < k \leq 0.94$, but the opposite holds for $0.94 < k < 1$.

For $\Omega = 1.8$, SRM is again the only detected mode of instability. Here ω increases again with k for both constant and variable applied fields. However, even though s for constant applied field increases again with k , s for variable applied field increases with k only if $0.08 < k < 1$ and decreases with increasing k in the small domain $0 < k \leq 0.08$. For constant applied field, s is larger than the corresponding one for the variable applied field if $0.18 \leq k < 1$, but the opposite is true if $0 < k < 0.18$. For constant applied field, ω is larger than the corresponding one for the variable field if $0 < k \leq 0.92$, and the opposite holds if $0.92 < k < 1$.

For $\Omega > 1.8$ and as Ω increases in this range, the domains in k for which s and ω for the constant applied field are larger than the corresponding s and ω for the variable field, decrease. It is also noticed that SRM favors constant applied field case, which corresponds to zero background charge density ($\sigma_0 = 0$), since the growth rate of disturbances for $\sigma_0 = 0$ is larger than the

corresponding one for $\sigma_0 \neq 0$ over most of range of values for k . In addition, SRM favors relatively larger values of k , where s for zero background charge density is larger than the corresponding one for non-zero background charge density.

For $\Omega = 2$, we still found that SRM is the only detected instability mode. Here ω increases again with k for both constant and variable fields. The growth rate also increases with k for constant applied field. However, for variable field, s increases with k in the range $0.32 < k < 1$ and decreases with increasing k in the range $0 < k \leq 0.32$. For constant field, s is larger than the corresponding one for the variable field in the range $0.28 \leq k < 1$, but the opposite is true in the range $0 < k < 0.28$. The frequency in the constant field case is larger than the corresponding one for the variable field if k is in the range $0 < k \leq 0.92$, while the opposite holds if k is in the range $0.92 < k < 1$.

For $\Omega = 2.375$, we found that for $\sigma_0 = 0.1$, in addition to SRM, which now exists for relatively larger values of k in the range $0.45 < k < 0.95$, we detected also a new mode, which is favored for relatively small values of k in the range $0 < k < 0.45$. Hereafter, we refer to this new mode of instability as spatial electric mode (SEM) since it turns that such mode is intensified with increasing the strength of the applied field. However, for zero background charge density, SRM is still the only instability mode for $0.05 < k < 0.95$. The growth rate of SRM for zero background charge density is found to be notably smaller than that for SEM, which exists for non-zero background charge density and in the domain $0 < k < 0.45$, while s for SRM of $\sigma_0 = 0$ is higher than the corresponding one for SRM of $\sigma_0 \neq 0$ if k is in the range $0.45 < k < 0.95$.

For $\Omega = 3$, both modes SRM and SEM exist for either $\sigma_0 = 0$ or $\sigma_0 \neq 0$. Typical results for s versus k and ω versus k for $\Omega = 3$ and for both $\sigma_0 = 0$ (solid line) and $\sigma_0 = 0.1$ (dashed line) are presented in Figures 2 and 3, respectively. It can be seen from the Figure 2 that for SEM, the growth rate for the variable applied field is larger than the corresponding one for the constant field. Detailed examination of the generated data for this figure indicates that for SEM and SRM, s for the variable field is larger than that for the constant field case if k lies in the ranges $0 < k \leq 0.84$ and $0.98 \leq k < 1$, respectively. However, for SRM, s for the constant field case is larger than that for the variable field case if k is in the range $0.86 \leq k \leq 0.96$. In addition, for SEM and the case of non-zero background charge density, s decreases with increasing k for $0 < k \leq 0.08$ and increases with k for $0.08 < k < 0.84$, while for SRM, s increases with k in the range $0.86 \leq k < 1$.

In the case of zero background charge density, for SEM, s decreases with increasing k in the small range $0 < k < 0.06$ and increases with k in the range $0.06 \leq k \leq 0.62$, while for SRM, s increases with k in the range $0.64 \leq k < 1$. It can be seen from the figure 3 that for SEM, the frequency for the non-zero background charge density is larger than that for the zero background charge density. In addition, for both SEM and SRM and for either constant or variable applied field, the frequency increases with k . Detailed examination of the generated data for this figure indicate that the frequency for constant field is smaller than that for the variable field case if k lies in the range $0 < k \leq 0.64$ or in the range $0.86 < k < 1$, while the opposite holds if k is in the range $0.66 \leq k \leq 0.86$.

For $\Omega = 3.3$, both SRM and SEM still exist. Detailed examination of the generated data for this case indicate that for variable applied field s increases with k for k in the ranges $0.06 < k \leq 0.74$ (SEM) and $0.84 \leq k \leq 0.90$ (SRM) and decreases with increasing k in either $0 < k \leq 0.06$ (SEM) or $0.76 < k < 0.84$ (SRM). For constant applied field, s increases with k in either $0 < k \leq 0.04$ (SEM) or $0.04 \leq k \leq 0.70$ (SEM) or $0.76 \leq k < 0.90$ (SRM). It is seen that the domain for SEM increases, while domain for SRM shrinks considerably. The growth rate for constant applied field is larger than that for variable field if k lies in either $0.76 \leq k \leq 0.82$ or $0.94 \leq k \leq 0.96$, while the opposite holds if k lies in $0 < k < 0.76$ or $0.82 < k < 0.94$ or $0.96 < k < 1$. For variable field, ω increases with k for either $0 < k < 0.74$ or $0.84 \leq k \leq 0.94$, while for constant field, ω increases with k for $0 < k < 0.70$ or $0.78 \leq k \leq 0.90$ or $0.92 \leq k \leq 0.96$. The frequency for the case of constant field is larger than the corresponding one for the case of variable field if k is in the range $0.80 \leq k \leq 0.82$ or $k = 0.96$, while the opposite holds if $0 < k \leq 0.78$ or $0.84 \leq k \leq 0.94$.

For $\Omega = 3.7$, only SEM exists. For the case of variable applied field, s increases with k for $0.06 < k \leq 0.94$ and decreases with increasing k in $0 < k \leq 0.06$, while for the case of constant field, s increases with k in $0.04 \leq k < 1$ and decreases with increasing k in $0 < k \leq 0.04$. The growth rate s for the case of variable applied field is larger than the corresponding one for the case of constant field if $0 < k < 0.96$, and the opposite holds for $0.96 \leq k < 1$. The frequency for the case of variable field is larger than the corresponding one for the case of constant field if $0 < k \leq 0.90$, while the opposite holds for $0.90 < k < 1$. For the case of variable field, ω increases with k in $0 < k \leq 0.94$ and decreases with increasing k in $0.94 \leq k < 1$. For the case of constant field, the frequency increases with k in $0 < k < 1$.

For $\Omega > 3.7$, SEM remains the only instability mode that the present spatial model predicts. Some typical results for s and ω versus k are shown in Figures 4 and 5, respectively, for variable applied field ($\sigma_0 = 0.1$) and for three values $\Omega = 1, 3$ and 4 . It can be seen from the figure 4 that the growth rate for SEM, increases with Ω , while the growth rate for SRM decreases with increasing Ω . In addition, for a given k , the growth rate for SEM is larger than that for SRM. We found that such results hold in general. It can be seen from the figure 5 that the frequency for SEM increases with Ω , while the frequency for SRM decreases with increasing Ω .

Figure 6 presents variations of the perturbation quantities versus axial variable for the spatial electric mode and for $\sigma_0 = 0.1$, $\Omega = 4$, $\omega = 0.1603$, $t = 1$, $k = 0.2$ and $s = 1.3921$. Due to the linear instability of the problem, we set $h' = 0.1$ and determined the other perturbation constants v' , σ' and E' using the procedure described in the previous section. The real parts of the perturbation quantities are used to collect the perturbation data for the instability mode for different values of z . It can be seen from this figure that most of the perturbation quantities begin to grow spatially after their generation at $z = 0$ and their spatial growth is seen mainly exponential type growth for values of z beyond $z = 5$ or so.

For $z > 7.5$, the amplitudes of the perturbations like v_1 and h_1 are sufficiently large that the present linear theory ceases to be valid. Figure 7 presents similar types of variations but for $\sigma_0 = 0$, $s = 1.2596$ and $\omega = 0.1381$. Again it can be seen that, for example, for $z > 6.5$, the amplitude of v_1 and h_1 are sufficiently large that the linear theory ceases to be valid. Comparing the results

shown in the figures 6-7, it can be concluded that spatial instability is more enhanced in the case of variable applied field.

4. Concluding remarks

Mathematical modeling and numerical investigation of linear spatial instabilities of electrohydrodynamic system for electrically forced slender viscous and finite conducting jet flows with externally imposed either constant or variable applied field were carried out. We were able to uncover two new instability modes one of which is enhanced with increasing the strength of the applied field, while the other one decays with increasing the strength of the applied field. In addition, it was found that the spatial instability modes are more effective in the case of variable applied field. However, the numerical results for the limiting case of very large conductivity ($K^* \geq 10^5$) for $\sigma_0 = 0.1$ that was compared well with the corresponding results for perfect conductivity case [Riahi (2009)], indicated the important role that the background surface charge density plays in the perfect conductivity case to suppress the spatial Rayleigh mode which was also noted in Hohman et al. (2001a) in the temporal Rayleigh mode of instability case.

The main results of the present study and predictions of the spatial Rayleigh mode and the spatial electric mode and their similarities on the way they depend on the strength of the applied field with the corresponding ones in the temporal instability counterpart [Hohman et al. (2001a)] for realistic and finite conductivity systems, indicate that both cases of the spatial instability on the neutral temporal stability boundary (present work) and the temporal instability on the neutral spatial stability boundary [Hohman et al. (2001a)] are subjected to the same types of instability mechanism. That is, the Rayleigh mode of instability driven by the surface tension is dominant if the externally imposed electric field is sufficiently weak, and the electric mode of instability driven by the electric field is dominant if the externally imposed field is sufficiently strong.

In regard to the relevance of the spatial instability modes for the jet flows, we note that for electrically forced jets, Hohman et al. (2001b) and Shin, et al. (2001) observed experimentally axisymmetric excitations and thickening blobs along the axial direction, and instabilities grew as they move downstream. These observations indicate presence of spatially growing disturbances in the jet flow. Although spatial instability modes can exist and operate even in the absence of the temporal instability modes as demonstrated in the present study, both temporal and spatial instabilities may operate independent of one another in the experimental and application cases.

As we referred earlier in the introduction section to the very recent analytical investigation by Riahi (2009), that work was for the restricted idealistic cases of zero or infinite electrical conductivity cases for electrically driven jet flows. Riahi (2009) considered spatial instability of such jet flows with variable applied field and under further restrictions on the frequency of the allowed disturbances. He found two spatial instability modes both of which were enhanced with increasing the strength of the externally imposed applied field. But, these two modes did not exist for disturbances with sufficiently small values of the axial wave number. However, in the present realistic case of viscous jet flows with finite electrical conductivity, we applied both modeling and numerical method for externally imposed variable or constant applied field to determine the growth rates of much wider class of disturbances, which were found to exist in

wider range of values of the axial wave number. In addition, the present results indicated that although one of the spatial mode of instability was enhanced with increasing the strength of the applied field, the other instability mode, which is classified as a spatial and electric analog of the well-known Rayleigh mode of temporal instability [Drazin and Reid (1981)], in fact decays with increasing the strength of the applied field.

Further extensions of the present study that are planned by the present authors to be investigated in future, are the cases of combined temporal and spatial instability case and spatial instabilities due to the non-axisymmetric disturbances. As is evident from the well known experiments by Taylor (1969) that the electrically forced jets can be non-axisymmetric and whip for sufficiently large values of the strength of the electric field, we can expect that spatial instabilities due to the non-axisymmetric disturbances can dominate over the axisymmetric ones if Ω is sufficiently large.

Acknowledgements

The authors would like to thank the referees for useful comments and suggestions that improved the quality of the paper. This research was supported by a 2008-2009 research grant from UTPA-FRC.

REFERENCES

- Anderson, D. A., Tannehill, J. C. and Pletcher, R.H. (1984). Computational Fluid Mechanics and Heat Transfer, Hemisphere Publishing Corporation, New York, N.Y.
- Baily, A. G. (1988). Electro-Static Spraying of Liquid, Wiley, New York, N.Y.
- Drazin, P. G. and Reid, W.H. (1981). Hydrodynamic Stability, Cambridge University Press, UK.
- Fridrikh, S. V., Yu, J. H., Brenner, M. P. and Rutledge, G.C. (2003). Controlling the fiber diameter during electrospinning, Phys. Rev. Lett., **90**, 144502.
- Healey, J. J. (2008). Inviscid axisymmetric absolute instability of swirling jets, J. Fluid Mech., **613**, 1-33.
- Hohman, M. M., Shin, M., Rutledge, G. and Brenner, M.P. (2001a). Electrospinning and electrically forced jets. I. Stability theory, Physics of Fluids, **13**(8), 2201-2220.
- Hohman, M. M., Shin, M., Rutledge, G. and Brenner, M.P. (2001b). Electrospinning and electrically forced jets. II. Applications, Physics of Fluids, **13**(8), 2221-2236.
- Li, D. and Xia, Y. (2004). Direct fabrication of composite and ceramic hollow nanofibers by electrospinning, Nano. Lett., **4**, 933-938.
- Lie, K. H. and Riahi, D.H. (1988). Numerical solution of the Orr-Sommerfeld equation for mixing layers, Int. J. Eng. Sci., **26**, 163-174.
- Melcher, J. R. and Taylor, G.I. (1969). Electro-hydrodynamics: A review of the interfacial shear stresses, Annu. Rev. Fluid Mech., **1**, 111-146.
- Michalke, A. (1965). On spatially growing disturbances in an inviscid shear layer, J. Fluid Mech., **23**, 521-544.

- Monkewitz, P. A. and Huerre, P. (1982). Influence of the velocity ratio on the spatial instability of mixing layers, *Phys. Fluids*, 25(7), 1137-1143.
- Rayleigh, L. (1879). On the instability of jets, *Proc. London Math. Soc.*, 10, 4-13.
- Reneker, D. H., Yarin, A. L. and Fong, H. (2000). Bending instability of electrically charged liquid jets of polymer solutions in electrospinning, *J. Appl. Phys.*, 87, 4531-4547.
- Riahi, D. N. (2009). On spatial instability of electrically forced axisymmetric jets with variable applied field, *Appl. Math. Modeling*, 33, 3546-3552.
- Shin, Y. M., Hohman, M. M., Brenner, M. P. and Rutledge, G.C. (2001). Experimental characterization of electrospinning: the electrically forced jet and instabilities, *Polymer*, 42(25), 9955-9967.
- Shkadov, V. Y. and Shutov, A.A. (2001). Disintegration of a charged viscous jet in a high electric field, *Fluid Dyn. Res.*, 28, 23-39.
- Soderberg, D. L. (2003). Absolute and convective instability of a relaxational plane liquid jet, *J. Fluid Mech.*, 439, 89-119.
- Sun, Z., Zussman, E., Yarin, A. L., Wendorff, J. H. and Greiner, A. (2003). Compound core-shell polymer nanofibers by co-electrospinning, *Advanced Materials* 15, 1929-1932.
- Tam, C. K. W. and Thies, A.T. (1993). Instability of rectangular jets, *J. Fluid Mech.*, 248, 425-448.
- Taylor, G. I. (1969). Electrically driven jets, *Proc. Royal Soc. A*, 313, 453-475.
- Yu, J. H., Fridrikh, S. V. and Rutledge, G.C. (2004). Production of sub-micrometer diameter fibers by two-fluid electrospinning, *Advanced Materials* 16, 1562-1566.

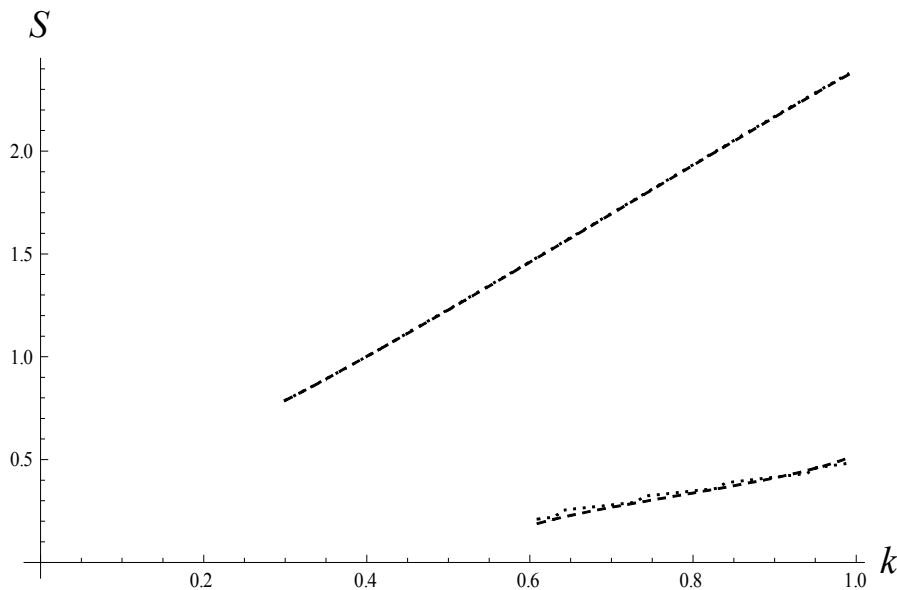


Figure 1. A comparison of the numerically computed results for the growth rate S versus the wave number k for very large conductivity $K^*=10^5$ (dotted lines) and the asymptotic results due to Riahi (2009) for $K^*=\infty$ (dashed lines). The values of the other parameters in this comparison are $\nu=0.333$, $\beta=77.0$ and $\sigma_0=0.1$.

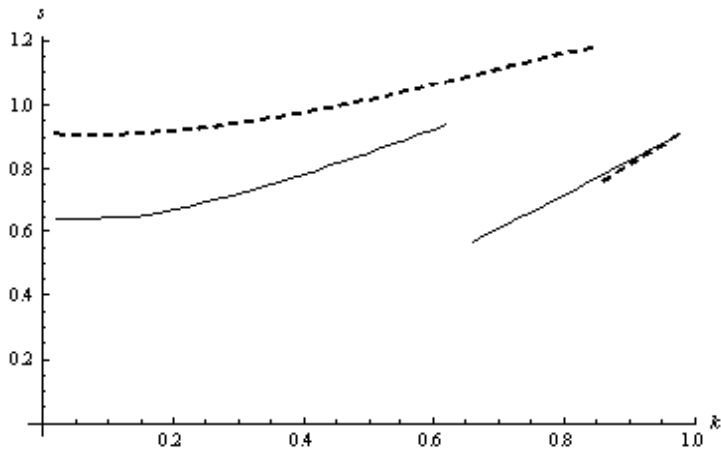


Figure 2. The growth rate s versus the axial wave number k for constant applied field (solid lines, $\sigma_0=0.0$) and for variable applied field (dashed lines, $\sigma_0 = 0.1$). Here, $K^* = 19.60$, $\nu^* = 0.61$, $\beta = 77.0$ and $\Omega = 3.0$.

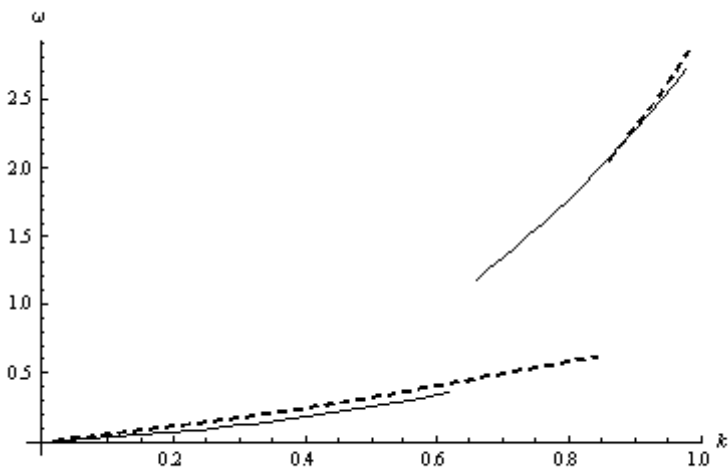


Figure 3. The same as in the figure 2 but for the frequency ω versus k

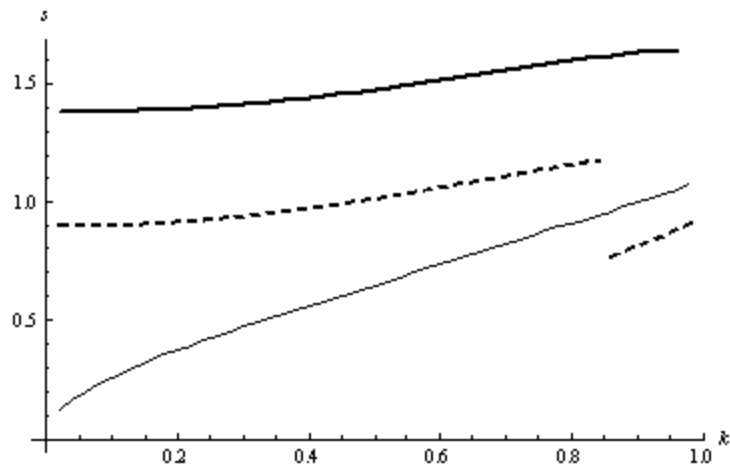


Figure 4. The growth rate s versus the axial wave number k for variable applied field for three values of $\Omega = 1$ (thin solid line), 3 (dashed line) and 4 (thick solid line).

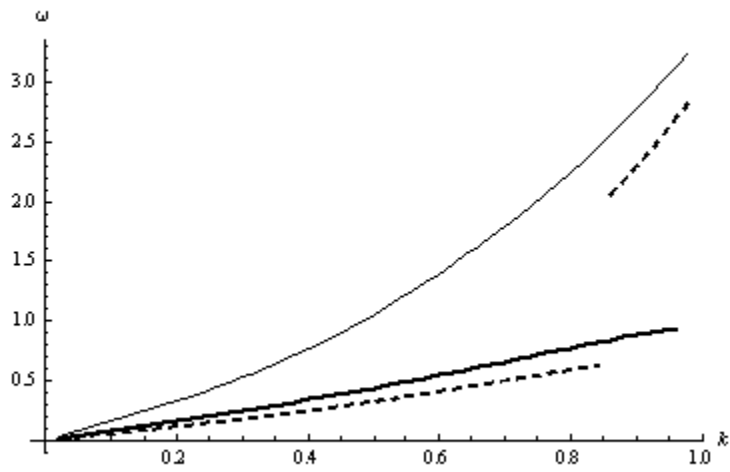


Figure 5. The same as in the figure 3 but for the frequency ω versus k

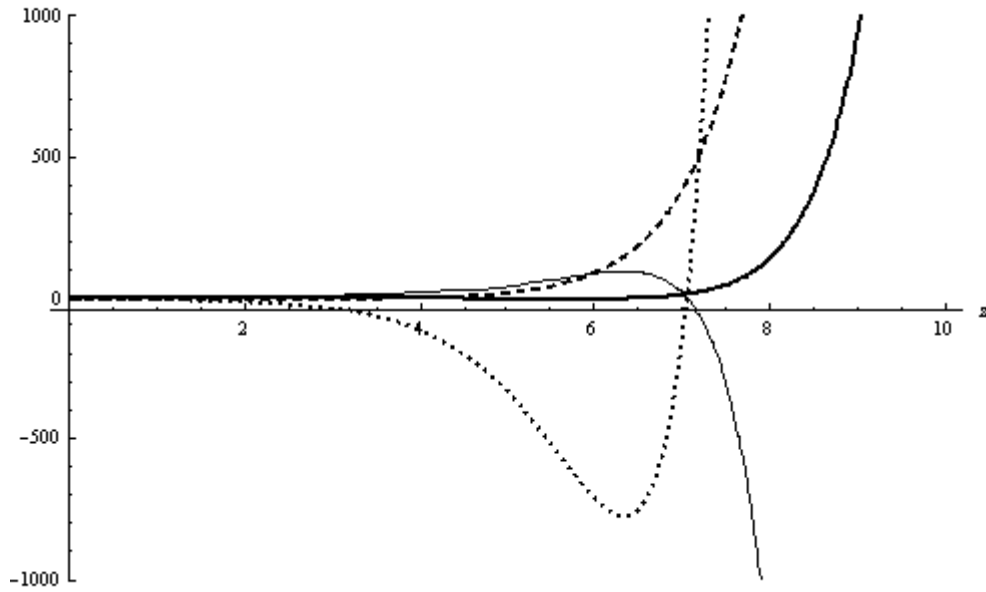


Figure 6. Perturbation quantities h_1 (thin solid line), v_1 (dashed line), σ_1 (thick solid line) and E_1 (dotted line) versus the axial variable z for $\Omega = 4$, $\sigma_0 = 0.1$, $t = 1$, $k = 0.2$, $s = 1.3921$ and $\omega = 0.1603$.

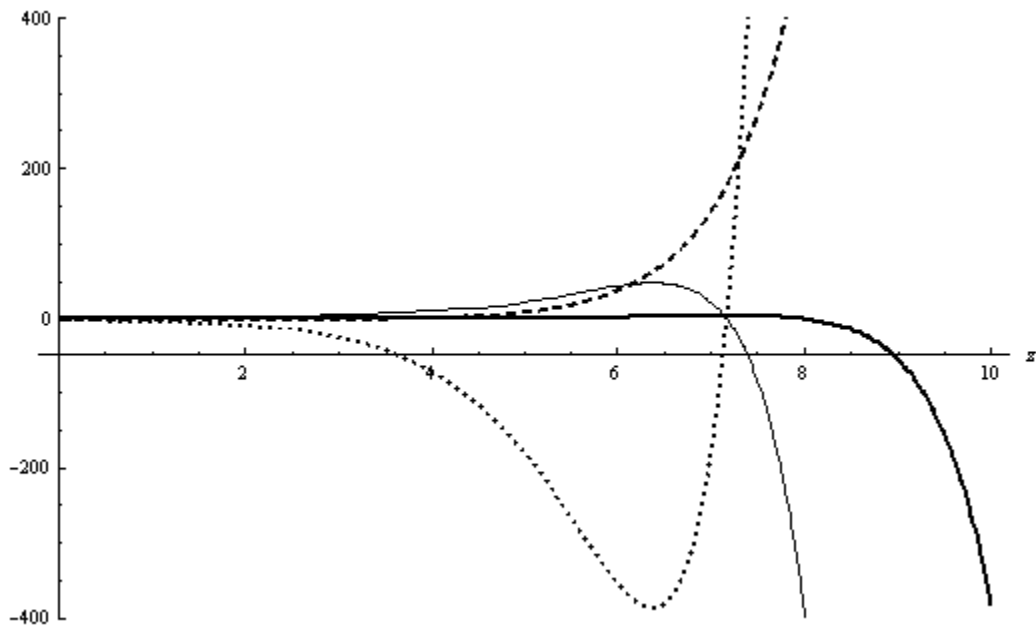


Figure 7. The same as in the figure 6 but for $\sigma_0 = 0$, $s = 1.2596$ and $\omega = 0.1381$.